

Chapter 5

The Physics of Extreme Sensitivity in WGM Optical Resonator Biosensors

5.1 Abstract

Whispering gallery mode (WGM) optical biosensors are capable of extraordinarily sensitive specific and non-specific detection of species suspended in a gas or fluid. Recent experimental results suggest that these devices may attain single-molecule sensitivity to protein solutions in the form of stepwise shifts in their resonance wavelength, λ_R , but present sensor models predict much smaller steps than were reported. This study examines the physical interaction between a WGM sensor and a molecule adsorbed to its surface, exploring assumptions made in previous efforts to model WGM sensor behavior, and describing computational schemes that model the experiments for which single protein sensitivity was reported. The resulting model is used to simulate sensor performance, within constraints imposed by the limited material property data. On this basis, we conclude that nonlinear optical effects would be needed to attain the reported sensitivity, and that, in the experiments for which extreme sensitivity was reported, a bound protein experiences optical energy fluxes too high for such effects to be ignored.

5.2 Introduction

Whispering gallery mode (WGM) optical microresonators have emerged as extraordinarily sensitive tools for the label-free detection of biomolecules in solution [60, 61, 81]. These devices employ a circular resonator made from a dielectric material, most often silica, and typically have diameters less than 200 μm . This results in an adaptable surface chemistry and small effective sensing area. These traits, along with their ability to detect unlabeled biomolecules, make WGM biosensors an appealing technology for the development of analytical and diagnostic instruments, but further development requires an understanding of how these devices function and the limits of their abilities.

Soon after the first application of WGM optical resonators as biosensors [5], researchers demonstrated stepwise shifts in the resonant wavelength, λ_R , upon exposure to nanoparticle [33, 105, 106, 107] and protein solutions [1, 108], suggesting single-molecule sensitivity for these species. This intriguing possibility has inspired efforts to reconcile these results [97] with the established model for sensor response presented by Vollmer and Arnold [5, 6]. However, that model implicitly assumes a linear optical response and approximates single-molecule contribution to the signal by extrapolating from response predicted for a full monolayer of material.

The adsorption of viral particles and polystyrene beads (200-750 nm diameter) were observed to produce shifts of 10–650 fm (10^{-15} m) in the resonant wavelength of spherical sensors[33, 105, 106]. It should be noted that these experiments may not fully represent molecular detection studies or be described by previous modeling efforts [5, 6] since the analyte is sufficiently large that it does not experience uniform electromagnetic field intensity upon binding. A later study by Lu et al.[107] investigated wavelength shifts in a toroidal sensor due to the adsorption of smaller (25, 50, and 100 nm diameter) polystyrene beads, reporting shifts of 0.4–11 fm. Although significantly smaller than the previously observed beads, these are still an order of magnitude larger than a single protein and too large to experience a uniform field. The greatest WGM sensitivity reported thus far is the 1–30 fm resonance shifts upon *specific* binding of the proteins Interleukin-2 and streptavidin (M_w 15.2 kDa and 60 kDa, respectively, and diameters < 5 nm) to toroidal sensors by Armani et al.[1, 108] using uniquely low-loss resonators and high coupled powers. The

details of published single-molecule or single-particle experiments involving the measurement of changes to λ_R that result from adsorption of these species are included in Table 5.1 along with abbreviations used to refer to these publications. Additional single-particle studies that measure quantities other than changes in λ_R [96, 109] are outside the scope of the present work since direct comparison is impossible.

This study examines the fundamental physical processes involved in the interaction between an optical WGM microresonator and material that adsorbs to its surface in an effort to understand the reported single-molecule sensitivity of these devices. We discuss the validity of assumptions made in previous efforts to model the behavior of WGM biosensors, and describe computational schemes necessary to capture the relevant physical phenomena. Finally, we apply these principles to predict sensor response according to computational capacity and available information about both the material properties and the experimental conditions and protocols employed in the different studies, and compare these results to data from single-molecule sensing experiments presented in SM1.

5.3 The WGM Biosensing Experiment

WGM optical resonators support circular modes that are confined to the periphery of the cavity via total internal reflection at the interface between the resonator and the surrounding medium. These modes are excited when the light introduced into the resonator can constructively interfere with itself by completing an integer number of optical cycles in the time required to make one revolution around the cavity. This occurs at the resonant wavelength, λ_R , which, assuming uniform properties around the entire resonator perimeter, can be expressed as

$$\lambda_R \approx 2\pi R_{mode}(T)n_{eff}(T)/M, \tag{5.1}$$

where M is the integer number of wavelengths in the cavity path length; T is temperature; R_{mode} is the effective radius of the mode; and n_{eff} is the effective refractive index of the mode (see Supplemental Information).

Total internal reflection at the resonator boundary produces an evanescent field in the medium outside

Table 5.1: Single-molecule and Single-particle Detection Using $\Delta\lambda_R$ for WGM Optical Biosensors

Code	Resonator		Analyte				λ (nm)	Q	P_D	$\Delta\lambda_R$ (fm)	Ref.
	Shape	Size ^a (μm)	Species ^b	Size ^c (nm)							
SM1	Toroid	$r_a = 40$ $r_i = 4$ d	Interleukin-2	< 5 nm	680	$1 - 2 \times 10^8$	≈ 1 mW	1 - 30	[9]		
SM2	Toroid	R = 45	Streptavidin	< 5 nm	680	d	d	2 - 30	[10]		
SP1	Sphere	R = 45	PSL ^e	200	1310	d	d	≈ 168	[5]		
			PSL ^e	500	1310	d	d	≈ 655			
			Virion (InfA)	≈ 50	765	6.4×10^5	d	11.4			
SP2	Sphere	R = 53	PSL ^e	750	1060	1.5×10^6	$32 \mu\text{W}$	≈ 500	[7]		
SP3	Sphere	R = 27	PSL ^e	500	633	1×10^6	d	≈ 550	[6]		
SP4	Toroid	d	PSL ^e	25	680	1×10^8	$10 \mu\text{W}$	≈ 0.35	[8]		
			PSL ^e	50	680	3×10^7	$10 \mu\text{W}$	≈ 0.5			
			PSL ^e	100	680	8×10^6	$10 \mu\text{W}$	≈ 11			
			Virion (InfA)	≈ 50	680	d	$10 \mu\text{W}$	1 - 11			

^aOuter radii (R) are given for spheres; major (r_a) and minor (r_i) radii are given for toroids

^bAll analytes are detected in aqueous solution

^cApproximate analyte diameter

^dInformation not provided by the authors

^ePSL: Polystyrene latex nanoparticle

the cavity. Material that binds to the device interacts with this electromagnetic field, altering λ_R in two ways. First, the adsorbed material displaces fluid, immediately changing the refractive index about the device. Second, the bound material absorbs energy, heating the surrounding device and fluid, causing their refractive index to change and the device to expand. The resultant resonant shift, $\Delta\lambda_R$, is described by [81]

$$\frac{\Delta\lambda_R}{\lambda_R} = \frac{\Delta n_{eff}}{n_{eff}} + \frac{\Delta R_{mode}}{R_{mode}} \quad (5.2)$$

Processes that alter either n_{eff} or R_{mode} , including the adsorption of material with a refractive index that differs from the medium surrounding the resonator, will result in a change in λ_R of a mode. The magnitude of the resonant shift increases with the contrast in refractive index between the adsorbed material and the surrounding medium it displaces, but sensitivity to single-molecule binding events requires that $\Delta\lambda_R$ exceed the measurement noise of the experiment, which was reported to be $\sigma_{\lambda_R} \approx 0.25$ fm in SM1.

Regardless of whether single molecule binding events are detected, WGM resonator sensors provide an extremely sensitive way to optically probe adsorbed species without measuring spectral features of the molecule or any tag that has been attached to it. Label-free techniques, such as this one avoid altering the behavior of the analyte molecule when attaching a tag, offering the opportunity to study the behavior of molecules in their native state. Detection of a specific analyte in a mixture may be accomplished by functionalizing the resonator surface with an antibody or other molecular recognition agent that binds exclusively to the species of interest. A variety of techniques have been reported for modifying silica surfaces [24].

The experiments leading to the reported single-molecule sensitivity of SM1 involved coupling approximately 1 mW of optical power into low-loss toroidal resonators, resulting in extremely intense electromagnetic fields within the cavity. This field strength is determined by the rate of energy coupled into the device and the rate of optical loss. The quality factor, Q , is the ratio of energy stored within the mode, W_{mode} , to the energy lost per optical cycle, and serves as a figure of merit for resonant cavities. This quantity may be expressed as $Q = \omega W_{mode}/P_D$, where P_D is the power dissipated by the cavity and ω is the resonant angular

frequency. At steady state, the power coupled into the device is equal to P_D . A high quality factor implies a resonator in which losses due to radiative mechanisms, absorption, or scattering are small[83, 110].

The studies reported in Table 5.1 span a wide range of experimental and optical parameter space. Two types of resonators were employed: (i) microtoroidal resonators were used in SM1, SM2, and SP4; (ii) microsphere resonators were used in the other studies. Some studies used narrow-linewidth 680 nm lasers to achieve the highest possible Q by minimizing absorptive losses in water, while others used lasers at 765 nm, 1060 nm, and 1310 nm. In all cases, the laser was coupled into the resonator via a tapered optical fiber waveguide. The coupled power used for experiments varied by at least two orders of magnitude from a high of $P_D \approx 1$ mW in SM1; this important parameter is, unfortunately, not uniformly reported in WGM resonator studies. Finally, the quality factor varied from $Q \geq 10^8$ (SM1,SP4) to $0.6 \times 10^6 < Q < 1.5 \times 10^6$ (SP1, SP2, SP3).

The variation in reported sensitivities may, at least in part, be a function of the differences in experimental and physical parameters involved. In the discussion that follows, we model WGM resonator sensor performance for the system for which the greatest sensitivity has been reported, i.e., SM1 [1]. In that experiment, the light transmitted through the waveguide was monitored with a photodetector while the wavelength was swept in a sawtooth pattern. None of the studies in Table 5.1 reported the scan rate; however, due to its importance, we obtained [2] the rate for SM1, $|\frac{d\lambda}{dt}| = 1.35$ nm s⁻¹. A Lorentzian dip in the transmission spectrum centered at λ_R indicated that light was coupled out of the waveguide and into a resonant mode, as illustrated in the simulated transmission spectrum in Figure 5.1 for a resonant mode in a device with a measured $Q \approx \lambda_R/\delta\lambda = 10^8$, where $\delta\lambda$ is the full width at half maximum of the resonance. The resonance shift, $\Delta\lambda_R$, is measured by first making a transient sweep with the sensor surrounded by fluid devoid of analyte. Transient sweeps are then taken continuously throughout the course of the experiment while a fluid containing analyte flows past the sensor. The difference between the initial resonance wavelength and the subsequent ones is the resonance shift. Although many more studies of WGM sensing have since been conducted, the combination of high Q (10^8) and coupled power ($P_D \approx 1$ mW) used in SM1 has yet to be repeated.

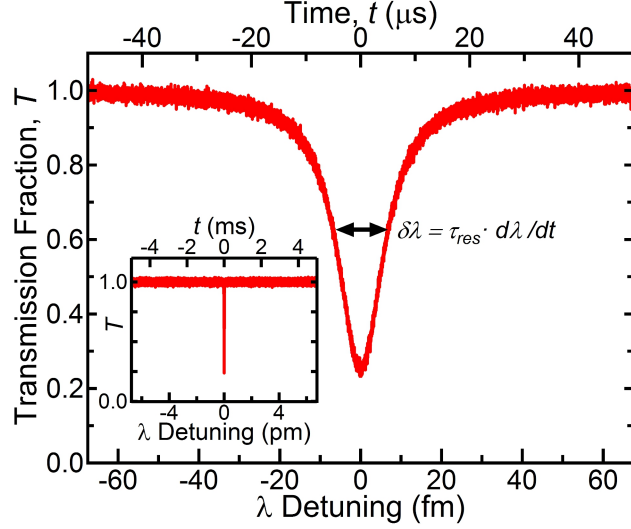


Figure 5.1: Part of a simulated transmission spectrum that might be observed by measuring the photodetector output using an oscilloscope while the wavelength is swept at $\frac{d\lambda}{dt} = 1.35 \text{ nm s}^{-1}$ across a resonance with $Q = 10^8$. The full wavelength scan is shown in the inset. The lower horizontal axis is in terms of wavelength detuning from λ_R while the upper is in terms of time.

5.4 Existing Models of WGM Biosensor Behavior

The first model to describe the WGM sensor response upon binding of protein molecules to its surface is presented by Arnold and Vollmer [6] and treats the bound material as a perturbation to the energy of the optical mode. The resulting shift in resonant wavelength is then expressed as

$$\frac{\Delta\lambda_R}{\lambda_R} \approx \frac{\delta W_{mode}}{W_{mode}} \approx \frac{\alpha_{ex} |\mathbf{E}_0(\mathbf{r})|^2}{2 \int \epsilon_R |\mathbf{E}_0(\mathbf{r})|^2 dV} \quad (5.3)$$

where W_{mode} is the mode energy, α_{ex} is the excess polarizability of the bound material (i.e., the difference in the polarizability of the protein compared and the water it displaced), $\mathbf{E}_0(\mathbf{r})$ is the electric field at position \mathbf{r} , ϵ_R is the permittivity of the resonator, and the denominator is integrated over all space. Applying the analytical solutions for the mode in a spherical device and integrating the effect of all molecules present at steady-state surface coverage provides an estimate of the frequency shift as a function of the surface density of bound proteins, σ_p , the refractive indices of the resonator and its surrounding medium, n_R and n_M ,

respectively, the permittivity of vacuum, ϵ_0 , and the effective radius of the mode, R_{mode} , i.e.,

$$\frac{\Delta\lambda_R}{\lambda_R} \approx \frac{\alpha_{ex}\sigma_p}{\epsilon_0(n_R^2 - n_M^2)R_{mode}}. \quad (5.4)$$

Teraoka, Arnold, and Vollmer [111] completed a more detailed examination of the effect of the protein on the electromagnetic field; they showed that Eq. (5.4) is the first-order perturbation term for the whispering gallery mode resonance.

This model assumes that perturbations to the optical properties of the mode that occur when protein molecules adsorb and displace solvent molecules are independent of the optical field strength. It also assumes that the magnitude of the energy perturbation this protein represents is limited to the difference in the work that must be done to distort the electron distribution of the protein to align with the electric field relative to the electron distribution of the solvent. The molecules are assumed to bind at randomly distributed positions on the sensor surface, a notion in need of validation in light of the subsequent demonstration of optical gradient forces trapping larger species (i.e., nanoparticles) in the evanescent field of a WGM resonator by the same researchers [111] and hydrodynamic focusing in the flowing-sample mode of operation employed in SM1 [112]. Nonetheless, this model is an excellent foundation upon which to advance our understanding of these devices. Experimental results presented by Vollmer et al. [5] and Arnold et al. [6] use resonators with $Q \approx 2 \times 10^6$ and unspecified coupled power to show that cross-sectional areas for bound proteins calculated from the measured $\Delta\lambda_R$ values agree well with crystallographic data.

The original inference of single-molecule detection with a WGM resonator in SM1 [1] presented a model to relate the resonance shift to intuitively important physical parameters. The authors noted that, at high circulating optical power, the effect of a bound molecule may be enhanced due to the thermo-optical effect, wherein the refractive index varies with temperature increases that occur as a result of light absorption by the bound molecule. This dependence is determined by the thermo-optical coefficient, $\frac{dn}{dT}$. The relative

single-molecule shift in resonant wavelength was estimated to be

$$\left[\frac{\Delta\lambda_R}{\lambda_R} \right]_{SM} = \frac{\sigma\lambda\frac{dn}{dT}}{8\pi^2n_R^2\kappa_TV}QP_D \int \frac{|u(\mathbf{r})|^2}{|\mathbf{r}| + \varepsilon} d\mathbf{r} \quad (5.5)$$

where σ is the absorption cross section of the protein, κ_T is the thermal conductivity of silica, V is the mode volume, $u(\mathbf{r})$ is the “whispering gallery mode field,” and ε is a size parameter on the order of the physical radius of the molecule. The model neglects thermal coupling between the resonator and the surrounding fluid, only considering temperature changes within the silica cavity where greater than 95% of the mode energy resides.

Though the authors provide no derivation for Eq. (5.5), it appears to have been inspired by the work of Gorodetskii and Il’chenko [113]. This study describes the heat generated by absorption in a differential volume element, h_V , in terms of the bulk absorption coefficient, α_{abs} , and the energy density of the electric field at that point, \tilde{W}_e , as $h_V = \omega\alpha_{abs}\lambda\tilde{W}_e/2\pi n$. Without a detailed derivation of Eqn. (5.5) it is difficult to identify and evaluate all the assumptions that went into the model, but the absence of any time-dependent quantity or heat capacity suggests that steady-state thermal conditions were assumed. Noting a three order of magnitude unit-conversion error in the absorption cross sections of the molecules studied by Armani et al.[1], Arnold[97] argued that this model cannot explain the wavelength shifts that were reported. Though the model appears to poorly describe the data, it suggests that nonlinear physical processes may contribute to the sensor response. If the bound protein causes heating, the strength of the heat source will vary with time as the wavelength is swept and P_D varies. The temperature plume generated by a single bound protein could, through this thermal perturbation, affect a region hundreds of times larger than the molecule itself. This phenomenon, also referred to as photothermal lensing, has been applied with great success to detect single molecules from changes in light scattering due to the thermal plume [114, 115].

More recently, Arnold et al. [97] consider the heat transfer to estimate the change in temperature experienced by the mode. They argue that the bound protein molecule can be treated as an induced dipole held in an electric field oscillating at frequency ω . The heat generated by the protein in watts, h , is then

expressed as the change in the energy of the configuration with time, a quantity that is related to the absorption cross section of the molecule via

$$h = \langle \mathbf{E}(\mathbf{r}_a, t) \cdot \partial \mathbf{p} / \partial t \rangle = \frac{1}{2} \omega \varepsilon_0 n_m \sigma |\mathbf{E}_0(\mathbf{r}_a)|^2 / k \quad (5.6)$$

where $\mathbf{E}(\mathbf{r}_a, t) = \mathbf{E}_0(\mathbf{r}_a, t) \exp(i\omega t)$ is the electric field at the position of the protein, \mathbf{p} is the induced dipole moment, \mathbf{r}_a is the position of the protein, ε_0 is the permittivity of vacuum, n_m is the refractive index of the medium surrounding the resonator, and k is the magnitude of the wave-vector in vacuum. This model describes the underlying physical processes that govern the steady-state response to a bound particle or molecule, but does not describe the transient signals produced by the swept-frequency experiments of Armani et al. [1] or any other researchers in the field. Thus, in spite of numerous efforts to model the extreme sensitivity of WGM biosensors, questions remain.

5.5 Physical Processes in WGM Sensing

Each of the aforementioned models incorporates simplifying assumptions in an effort to develop analytical descriptions of WGM biosensor resonance shifts. The discussion that follows explores the physical processes in an effort to develop a model that more accurately describes the the experimental system for which extreme sensitivity has been reported.

First, we consider the nature of the WGM sensing experiment. As noted above, the simplest models assume that the laser is continuously tuned to the resonance to enable steady-state operation despite this setup never having been demonstrated experimentally [116]. In contrast, the experiments of Table 5.1 involve sweeping the laser output over a range of wavelengths to find resonance. To capture the widest variety of physical phenomena that may occur using this technique, we model experiments at high P_D and Q . Nanoparticle studies are thus irrelevant to the model under development since there no high-power, high- Q studies to compare with the model. As a result, we consider the single-molecule studies SM1 and SM2.

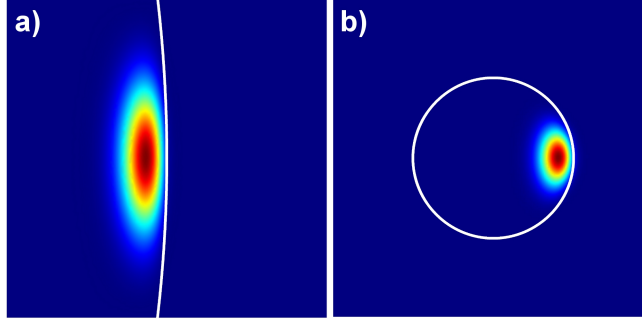


Figure 5.2: The normalized mode intensity for $\lambda_R \approx 680$ nm in a (a) spherical ($R = 42.5 \mu\text{m}$) and (b) toroidal ($r_a = 40 \mu\text{m}$, $r_i = 2.5 \mu\text{m}$) WGM resonator.

Excitation of the Optical Mode

Whispering gallery modes may be excited in a variety of closed dielectric structures including rings, disks, spheres, cylinders, tubes, and toroids [60, 61]. Each of these geometries has unique mode structures, as illustrated in Figure 5.2 for spherical and toroidal cavities. Predicting how biomolecules that adsorb to the surface of these devices will interact with resonant light begins with an accurate description of this mode structure.

Light is coupled into the microcavity using a waveguide, which we assume here to be a tapered optical fiber waveguide as described above. An evanescent wave decays with distance from the surface of the waveguide; bringing the resonator within the evanescent field couples a traveling wave into the cavity. The extent to which the optical field from the waveguide overlaps the WGM in the resonator determines how much total power can be coupled into the device [88]. Previous studies ignore the method of coupling and assume that a single mode is populated in the WGM resonator [97]. This choice does not necessarily reflect experimental conditions as modes often overlap in wavelength-space, but it appears to be an acceptable approximation. Spherical and cylindrical cavities provide the advantage of well-developed analytical expressions for the electric and magnetic field profiles [89, 117] for a variety of coupling methods. Oxborrow [103] presented a convenient, and much more general, method for calculating the mode profile for axisymmetric systems using COMSOL multiphysics, the same finite element solver that we employ below. The numerical solutions obtained via this method must, however, be rescaled to reflect the power coupled into the cavity for a given

experiment. Another approximate expression for the mode in a toroid was derived using perturbation theory for quasi-TE and TM modes [80], although those expressions are not provided in their entirety.

Poynting's theorem for harmonic fields may be used to calculate the energy flux inside and outside of the resonator. In the case of no current flow, this is

$$2i\omega \int_V (\tilde{W}_e - \tilde{W}_m) dV + \oint_A \mathbf{S} \cdot \mathbf{n} da = 0, \quad (5.7)$$

where $\mathbf{S} = \frac{1}{2}(\mathbf{E} \times \mathbf{H}^*)$ is the time-averaged Poynting vector, \mathbf{n} is the unit normal vector at the differential surface da , \mathbf{E} is the electric field, \mathbf{H} is the auxiliary field, and \tilde{W}_m is the energy density of the magnetic field. The first term in this expression is integrated over the volume of the system and the second term is integrated over the surface area of the system.

For a resonator fabricated from a lossless dielectric, and with no scattering at the resonator boundaries, $\oint_A \text{Re}(\mathbf{S} \cdot \mathbf{n}) da = 0$ because there would be no net energy flow leaving the cavity for such an ideal device. The imaginary part of the Poynting vector for this system is a measure of the circulating, or stored, energy. The materials used in the laboratory are far from ideal, each with its own complex refractive index, so power will be coupled out of the resonator according to the real part of the Poynting vector as scattered and absorbed light. The time-averaged Poynting vector incorporates all the losses due to scattering and heating within both the glass and the surrounding water. It does not include the additional losses due to the perturbation of the system by the protein; these must be evaluated using the light remaining in the resonator ($\text{Im}(\mathbf{S})$). This is similar to the attenuation of circulating power in a resonator by a point defect [118]. A typical value for the time-averaged energy flux at the surface of a microcavity with $Q \approx 10^8$ and $P_D \approx 1$ mW is $1-10 \times 10^{13}$ W/m².

Since the excitation wavelength is scanned during the measurement of the transmission spectrum, the power coupled into the WGM changes as a Lorentzian function of time as the wavelength is scanned at rate $\frac{d\lambda}{dt}$ past the resonance (see Fig. 5.1). For the single-molecule experiments in Table 5.1, the typical time required for optical loss mechanisms and the "ring-up" of the mode to reach a steady state ($\tau_{WGM} < 10$ ns)

is very small compared to both the total time for a wavelength scan ($\tau_{scan} \approx 5$ ms) and the time to scan across a single resonance of $Q \approx 10^8$ ($\tau_{res} \approx 5$ μ s based on full width at half-maximum of Lorentzian profile). This useful relationship, which may be expressed as $\tau_{WGM} \ll \tau_{res} \ll \tau_{scan}$ suggests that optical timescales may be considered instantaneous.

Interaction of Resonant Light with Surrounding Materials

Here we consider the interaction between the electromagnetic fields in a resonator with $Q \approx 10^8$ and the various materials that play a role in a WGM sensing experiment. As light passes through matter, the time-varying electromagnetic fields interact with the electrons in a material according to its molecular or crystal structure. A single molecule, for example, may have a net dipole moment if it includes net charge or an asymmetric arrangement of atoms with varying electronegativities. Regardless of whether such a permanent dipole exists, an electric field will distort the flexible electron distribution in a material and generate an induced dipole according to the polarizability of the molecule. These dipoles will align themselves to the instantaneous orientation of the electric field. The interactions between light and matter result in a slower propagation than in a vacuum, and are collectively described by the complex refractive index $\tilde{n} = n + i\kappa$. The real part of the refractive index, n , is the ratio of the propagation velocity in vacuum, ν_{vac} , to that in a particular material, ν_{mat} , i.e., $n = \frac{\nu_{vac}}{\nu_{mat}} = \frac{\lambda_{vac}}{\lambda_{mat}}$. The imaginary part of the refractive index, κ , describes the attenuation of light due to loss mechanisms such as absorption or scattering.

Regardless of whether a protein molecule is present, light circulating within the WGM resonator interacts with the silica cavity and the water surrounding the device. Water molecules form strong hydrogen bonds with one another. The electron distribution in each material undergoes oscillating perturbations in response to the optical field. Water molecules, however, are free to alter their orientation to the extent allowed by their hydrogen bonds. In contrast, silica exists as a rigid amorphous solid whose covalent bonds prohibit any significant translational or rotational motion. The energy that induces this electron and molecular motion is dissipated as heat, leading to linear absorption by these materials in the electromagnetic field.

The presence of a bound protein molecule on the surface of the resonator complicates this response. Each

of the amino acids in a protein molecule has a unique permanent dipole moment and molecular polarizability that reflects its composition. Exposure to an electric field induces an additional dipole moment, just as in the silica and water, but the protein can also change its conformation in response to the applied field. The tertiary structure of the protein is determined by the intramolecular forces as well as the energetic incentive to hide hydrophobic regions of the molecule from the surrounding water. What is often thought of as a rigid molecule is, in fact, in continuous flux. Thermal vibrations allow the molecule to sample a range of conformations, all of which are sensitive to interactions with surrounding species and external electric fields. Each conformation has a unique permanent dipole moment, however. Whereas the permanent dipole moment can be treated as a constant for silica and water, this flexibility causes the molecular conformation, induced dipole moment, and permanent dipole moment of the entire protein molecule to become functions of time in the presence of intense, temporally, and spatially varying electric and magnetic fields.

The behavior of the protein in these conditions is even more complex when considering the non-ideality of the interactions between light and matter. It is useful at this point to view the protein as a network of oscillators (i.e., polarizable amino acids) being forced by time-varying optical fields. The timescale of the variation of the electric field ($\tau_{field} \approx 10$ fs) is much shorter than that of molecular motion[119] ($\tau_{molecule} \approx 10$ – 1000 fs), so there is a lag between the instantaneous alignment of the field and the orientation of the permanent dipole. In contrast, induced dipoles are established in time $\tau_{electron} \approx 10^{-3}$ fs \ll τ_{field} . The existence of a lag in the alignment of the permanent dipole implies that the electric field must fight the rotational momentum it imparted on the protein during its last optical cycle, increasing the energetic cost as light propagates through the protein. We refer to the work required to align the induced and permanent dipoles as W_A ; it depends on protein size, permanent dipole moment, and the polarizability of the constituent amino acids. Only the portion of this work related to the creation and alignment of the induced dipole is considered by Arnold and Vollmer[5, 6].

The conformational changes that the protein undergoes may give rise to an additional lag between the orientation of the protein dipole and the electric field alignment. In this case it is more reasonable to view the protein not as a molecule, but as a polymer where each amino acid is responding independently. The

3-dimensional arrangement of these components reflects a vast array of intramolecular interactions that are stretched and bent when an electric field is applied to the molecule. Behaving like springs, these interactions can oppose molecular realignment and increase the amount of work that must be done by the optical fields, W_{IM} . The calculation of W_{IM} based on amino acid sequence or a known tertiary structure has yet to be demonstrated.

Finally, an accurate molecular-scale depiction of the protein must also include the thermal motion that constantly perturbs the tertiary structure of the molecule. The electric field must fight the thermal vibrations of the protein molecule as it changes its conformation. Since each amino acid responds differently to the field according to its physical properties and interactions with nearby amino acids, the degree of thermal vibration is likely nonuniform across the molecule. An electric field must overcome the thermal energy of the system ($E_{thermal} \approx k_B T$, where k_B is the Boltzmann constant) in order to maintain alignment of the dipoles. Therefore, thermal effects could be significant at high optical intensities because of increased absorptive heating, thereby increasing the work to overcome thermal motion, W_T .

The total work done by the propagating optical field on a protein molecule, W_{tot} , may be thus expressed in terms of these three sources

$$W_{tot}(T) = W_A + W_{IM} + W_T(T) \quad (5.8)$$

where W_A describes the work to overcome the forces resulting from a lag in alignment between the electric field and the protein dipole, W_{IM} is the work required to overcome intramolecular forces that introduce additional lag, and W_T is the work done correcting for misalignment due to thermal vibrations. This work is dissipated as heat when the field imparts kinetic energy on the molecule, and that energy is transferred to the surroundings via molecular collisions.

Energy may also be injected into the system as heat if the protein directly absorbs light. Absorption requires the incident light to be at a frequency that excites mechanical or electronic resonances in the molecule. At low optical intensities, the amount of heat generated is proportional to the amount of light absorbed. This process is typically described by the absorption cross section of the molecule, $\sigma(\lambda)$, which is

the cross section that a black body absorber would have if it was absorbing as much light as the protein. The absorption cross section of a protein in solution may be calculated based on absorbance measurements in the dilute limit (where scattering and agglomeration may be neglected). Typically, non-fluorescent proteins do not absorb strongly near 680 nm (in contrast to $\lambda < 350$ nm where proteins absorb quite efficiently due to the electronic structure of aromatic amino acids). As a result, concentrations above 10 μ M must be used for these absorption spectrophotometry measurements despite the potential for artifacts such as aggregation that may occur at such high concentrations.

The intense optical fields that build up within a WGM resonator with $Q \approx 10^8$ (irradiance $\approx 10^{13}$ W/m²) suggest that linear absorption may account for only a portion of all energy that is absorbed by a surface-bound protein molecule and consequently dissipated as heat. To date, the contribution of nonlinear phenomena to WGM sensor response has been ignored, but it may be relevant due to the high irradiance experienced by adsorbed material. In fact, the intense circulating powers achievable in WGM resonators have been used to create lasers by doping the dielectric with a gain medium [120, 121, 122]. An important category of nonlinear effects is optical limiting, which is often studied in chromophores [123, 124] with respect to optical limiting switches and other photonic applications[125, 126]. This phenomena is characterized by a significant deviation from linear absorption behavior with increasing irradiance. Optical limiting of transmission is often explained by phenomena such as multiphoton absorption, a process involving absorption of an additional photon by a molecule that is already in an excited state. A large irradiance, and the frequent photon interactions that result, are necessary to exceed the threshold at which an additional photon arrives during the lifetime of the excited state. One can imagine that, even for meager absorption, exposure to a sufficiently high power of light would increase the vibrational energy of the protein molecule greatly and may vastly increase the amount of work required to overcome W_T .

Other nonlinear optical phenomena may play a role in WGM sensing as well, including second harmonic generation (SHG) and the Kerr effect. SHG is a second-order nonlinear process that involves the generation of light at $\lambda_{SHG} = \frac{1}{2}\lambda_{input}$, which, for the excitation wavelengths used in WGM biosensing experiments ($\lambda_{input} = 680$ nm), generates light in a range that is absorbed *far* more efficiently (10x or more) by proteins

than the WGM excitation light. SHG is more likely to occur at a material interface because inversion symmetry is broken there [127], enabling a weak SHG signal to be generated even in materials such as silica that do not exhibit the phenomena in the bulk [127]. This technique was recently used to demonstrate coherent SHG from a small number of fluorescent molecules patterned on a spherical WGM resonator [128]. The Kerr effect, which is a third-order nonlinear process whereby the refractive index of a material is a function of the electric field strength, has been demonstrated relevant in silica for ultra-high Q resonators at room temperature [129].

Unfortunately, very little information is available on the physical constants describing nonlinear phenomena in non-fluorescent proteins. If a fluorescent species absorbs efficiently, its binding could cause both a resonance shift *and* a step change in the quality factor of the mode [1]. Non-fluorescent species absorb too little light to measure these physical properties using conventional fluorescence spectroscopy. Although it is difficult to generate continuous electromagnetic waves intense enough to probe nonlinear optical phenomena for proteins, ultra high Q WGM resonators generate the needed fields, possibly contributing to the previously reported sensitivities and enabling future study of nonlinear phenomena in biomolecules. Thus, the uv-vis spectrophotometric measurements used to describe simple, linear absorption are likely incomplete.

Heat Transfer

A non-fluorescent protein molecule that absorbs light will generate heat $h = \sigma \text{Im}(\mathbf{S} \cdot \hat{\phi})$, where $\hat{\phi}$ is the unit vector in the direction of light propagation. A fluorescent protein dissipates some of its absorbed energy as light, however the remainder is converted to heat according to $h_f = (1 - \eta_q)h$, where η_q is the quantum efficiency of the fluorophore under experimental conditions. The dissipated heat will be removed from the vicinity of the absorbing protein(s) by collisions with surrounding molecules. The thermal coupling of the protein to the resonator and to the surrounding fluid depends on the molecular configuration, which includes a patchy network of hydrophobic and hydrophilic regions, in contrast to the uniform surfaces of polymer beads that have been the subject of numerous studies (see Table 5.1). Recent molecular simulation studies suggest that these local regions of hydrophobicity in the protein can decrease the density of the surrounding

water molecules immediately adjacent to those regions, drastically reducing the ability of the protein to transmit its thermal energy to the solvent [130].

Furthermore, in specific binding studies, the protein is not bound directly to the surface of the resonator. Instead, it is tethered to the resonator by the targeting species, which itself has been immobilized to the surface, possibly through covalent linkages. These molecular recognition agents that connect the protein to the resonator surface further differentiate the biomolecule sensing experiments from those involving beads. This may mean that, in the case of the protein, the most efficient means of dissipating energy could be through the high-affinity interactions with the targeting molecule attached to the sensor surface. This could have significant implications on the isotropy of heating that occurs in response to excitation of the protein by the resonant light, suggesting that the molecular properties of the targeting molecule (e.g., rigidity, polarizability, size, etc.) could play a role in the resonance shift observed upon analyte binding. To date, researchers have assumed that the interaction between the targeting species and the mode contributes only to the baseline of the resonance shift measurement and plays no role during the analyte sensing experiment.

The modeling of nanoscale heat transfer requires knowledge about these numerous and complex interactions between a particular protein species and its surroundings [131]. Lacking the data to describe these molecular-scale effects, we assume bulk material properties and energy transport models that apply to macroscopic systems. This assumption is quantitatively accurate within the silica and water, describing the formation of a temperature plume with characteristic radius $l_{plume} \sim (\rho C_P \tau_{res} / \kappa_T)^{-1/2}$, where ρ is the material density and C_P is the heat capacity. There is a transition from a discrete to a continuous system near the protein molecule that will affect the magnitude of the temperature perturbation within this plume and, ultimately, determine the magnitude of the resonance shift. Heat transfer in the continuous system may be described by the heat conduction equation,

$$\mathbf{q} = -\kappa_T \nabla T, \tag{5.9}$$

where the heat flux \mathbf{q} is proportional to the local gradient in temperature. The energy balance for the WGM

biosensor system may be expressed as

$$\rho C_P \frac{dT}{dt} + \kappa_T \nabla^2 T = \frac{\omega \alpha \lambda n |\mathbf{E}|^2}{2\pi} + h_{SM} \delta(\mathbf{r} - \mathbf{r}_a), \quad (5.10)$$

where the transient temperature profile, $T(\mathbf{r}, t)$, is evaluated at position \mathbf{r} and time t . All physical properties are a function of \mathbf{r} to account for the different materials. The right side of (5.10) describes heat generation in the system. The first of these terms describes the heat source due to bulk absorption by the resonator and its surroundings [113], while the second term represents that due to the protein at position \mathbf{r}_a . Here δ represents the Dirac delta function. In these experiments the protein sits at the interface between two materials, and so thermal dissipation will be anisotropic due to the different physical properties in the resonator and the surrounding fluid (see Supplemental Information). Note also that the magnitude of the electric field, $|\mathbf{E}(\mathbf{r}, t)|$, is a function of position *and* time because the power is coupled into the resonator in a Lorentzian time pulse (as illustrated in Fig. 5.1) as the wavelength is swept past the resonance.

This Lorentzian functional form represents an ideal case. The true shape of this function is a challenge to predict *a priori* because it can be strongly affected by bulk heating due to absorption, but the Lorentzian shape and its distortion have been modeled for axisymmetric systems[132]. As the wavelength is swept, absorption warms the resonator and surrounding medium, causing a shift in the resonant wavelength according to the thermo-optical effect. Since their thermo-optical coefficients have opposite signs, the warming of water will produce a resonance shift opposite in sign to that caused by warming silica. This results in an asymmetric broadening or narrowing of the resonance peak in the transmission spectrum depending on that fraction of the mode that overlaps each material [1] or the direction of the wavelength sweep (see Supplemental Information). This effect, discussed in further detail by Carmon, et al. [116], was also observed by Lu and colleagues in SP4 for $P_D \approx 10 \mu\text{W}$ and is experimentally demonstrated in the Supplemental Information to this chapter. One consequence of this heating effect is that the up scan has a wider resonance peak, which allows power to be coupled in for a longer fraction of the scan, possibly increasing sensitivity. What appears to be a Lorentzian peak in the case of negligible absorption can become a complex function of the

material properties and experimental parameters. Schmidt et al. [133], and Rokhsari et al. [134] explore in more detail the role of $\frac{d\lambda}{dt}$ and P_D on the appearance of the transmission spectrum. Transmission curves from biosensing experiments are rarely, if ever, reported. This handicaps efforts to validate any model, as these curves are needed to accurately gauge distortion by bulk heating, and the subsequent effects on coupled power throughout the experiment.

The thermal effects that contribute to the distortion of the Lorentzian transmission peak used to identify the instantaneous value of λ_R in a WGM biosensing experiment emphasize the transient nature of the experiment. A measurement with time resolution of τ_{scan} is used to determine a quantity that varies on a timescale τ_{res} . By considering thermal diffusion, we introduce another timescale: the time for a heat source at the sensor surface to be experienced by the optical mode, τ_{HT} . This timescale may be expressed in terms of material properties and the relevant length scale over which diffusion must occur, l_{mode} . We assume that the radial distance from the sensor surface to the peak of the mode intensity as an acceptable approximation of l_{mode} , which gives $\tau_{HT} \approx \frac{r_{a\rho}^2 C_p}{\kappa_T} \approx 0.3 \mu s$ for the toroidal resonators used in SM1. This value is comparable to τ_{res} , implying that it will take the duration of the pulse before the entire mode experiences the full effect of the heat from a single-molecule source. Our efforts to solve the transient Equation (5.10) represent a significant deviation from previous efforts to model WGM biosensor response [5, 6, 111, 1, 97] where no heating or steady-state heating are assumed.

Changing Material Properties

It is evident from the analysis of molecular scale physical processes that no previous effort to describe the WGM sensor device response has modeled the transient sensing experiment in which attomolar sensitivities and single-molecule binding events were observed. By scanning the excitation wavelength in order to measure λ_R , the power coupled into the optical field becomes a function of time and position \mathbf{r} . Both linear and nonlinear optical phenomena introduce heat into the system, making the temperature a function of position and time t as well. The electric field and temperature change with time; so too will a number of important physical properties of the system. These include the refractive index and thermo-optical coefficient [135],

Table 5.2: Summary of Functional Dependencies of Physical Properties

Refractive Index	$n(T, \mathbf{E} , \mathbf{r})$
Resonator Radius	$R_{res}(T)$
Bulk Absorption Coefficient	$\alpha_{abs}(T, \mathbf{E} , \mathbf{r})$
Protein Absorption Cross Section	$\sigma(T, \mathbf{E})$

absorption coefficient, and protein absorption cross section. The resonator may also expand due to bulk temperature increases on the order of 1-10 K according to the thermal expansion coefficient [116], α_{exp} . These effects are summarized in Table 5.2. At the level of the individual protein and its surroundings, any application of bulk material properties may be quite inaccurate due to local variations in density or energy.

5.6 Modeling WGM Biosensors

A rigorous model of the transient WGM biosensing experiment must take into account all of the physical processes outlined above, including the time-varying material properties of the system. Calculating the sensor response, $\Delta\lambda_R(t)$, therefore requires a numerical computation scheme like the one depicted in Fig. 5.3a, which involves evaluating the instantaneous value of λ_R at discrete points in time. In this case, accuracy demands that the time steps be sufficiently small to capture the rapid changes that occur in the system due to the Lorentzian shape of the curve in Fig. 5.1. In general, solving for $\Delta\lambda_R(t)$ requires beginning at $t = 0$ and continuing by: (i) evaluating the power coupled into the resonator based on $\lambda(t)$, (ii) determining the material properties of the system as a function of current temperature profile and position, (iii) calculating the 3-dimensional electromagnetic field profile, (iv) evaluating the amount of heat generated by the silica, water and protein according to the electromagnetic field profile, (v) solving for the updated temperature profile, taking into account thermal diffusion, (vi) calculate integral

$$\Delta n_{eff} \approx \frac{\int_V \frac{dn}{dT} \Delta T(\mathbf{r}) |\mathbf{E}(\mathbf{r})|^2 dV}{\int_V |\mathbf{E}(\mathbf{r})|^2 dV} \quad (5.11)$$

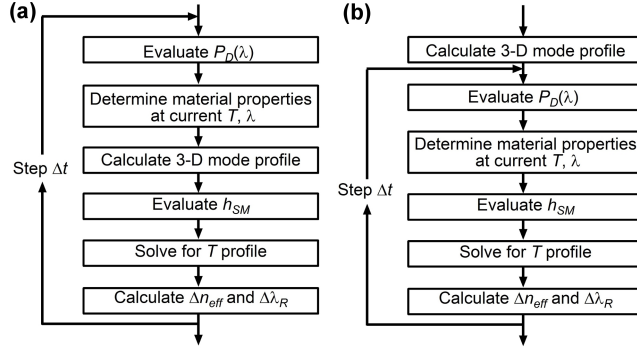


Figure 5.3: (a) Rigorous and (b) modified computation schemes for calculating the WGM sensor response.

to determine $\Delta\lambda_R$, and (vii) stepping Δt in time and repeating this process. A more complete discussion of this computation method is included in the Supplemental Information.

Simulating all simultaneous physical processes using the scheme in Fig. 5.3a is not presently possible due to the lack of information about how a single protein molecule may respond to the intense optical fields within a WGM resonator with $Q \approx 10^8$. We instead begin by evaluating the assumptions that may be made to simplify this enormous challenge. For example, thermal expansion due to temperature change may be considered negligible according to both theoretical predictions and experimental observations [136], suggesting that we may be able to omit the second term on the right hand side of Eq. 5.2. However, it remains unclear if the thermal perturbation from the protein heat source is significant enough to warrant repeating the mode structure calculation at each computation step in light of the local thermal expansion of the silica that may result. The full, 3-dimensional simulation of the mode structure and solution for the eigenfrequencies (i.e., resonant frequencies) of the mode, followed by the evaluation of the protein heat source and solution of micro-scale heat transfer, would accomplish the same goals as the computation scheme above, but would require a supercomputer to implement.

Finite element analysis has become a valuable tool in solving for such complex systems, and it is particularly well-applied here where computational accuracy and labor can be focused on regions in the geometry where it is needed by generating smaller mesh elements there. We use a commercially available software package, COMSOL Multiphysics, to solve for the electromagnetic field and the temperature profiles, as a

function of time in the simple case of a point source of heat at the interface of silica and water blocks.

Here we used the computation scheme outlined in Fig. 5.3b to consider the limiting case where the only heat introduced into the system is due to linear absorption by the protein molecule during a frequency sweep, and the effect that this thermal perturbation has on the mode structure are negligible. These assumptions are identical to those made in previous evaluations of the thermo-optical model of WGM biosensor response [1, 97], but our efforts include a consideration of transient heat transfer. We use the Oxborrow method [103] to calculate the electromagnetic field profiles for a toroidal resonator with major radius $r_a = 40 \mu\text{m}$, minor radius $r_i = 2.5 \mu\text{m}$, and material properties as detailed in the Supplemental Information. We also assume that the analyte is the common tetrameric protein streptavidin[97] ($M_w \approx 60 \text{ kg/mol}$) for which $\sigma = 1 \times 10^{-23} \text{ m}^2$. At peak coupled power the protein molecule is exposed to an irradiance of $6 \times 10^{13} \frac{\text{W}}{\text{m}^2}$ and produces a heat of $h_{SM} = \sigma \text{Im}(\mathbf{S} \cdot \hat{\phi}) \approx 6 \times 10^{-10} \text{ W}$. Quality factors ranging from 10^6 to 10^8 are also considered.

5.7 Results and Discussion

We model the WGM biosensor response to the adsorption of a single protein molecule, as in SM1, using the computational scheme outlined in Fig. 5.3b to solve for the mode structure, the intensity of the single-molecule heat source, and the 3-dimensional transient temperature profile. The results of our finite element model show an asymmetric thermal plume that evolves and expands over time into the silica and the water. A cross-section of the temperature profile at peak coupled power, as well as its overlap with the mode structure, is depicted in Figure 5.4. To better visualize the transient evolution of the plume, we look more closely at the temperature at two points of interest in Figure 5.5. These two points correspond to the location of the protein and the point of maximum mode intensity. Note that the maximum temperature that occurs at the mode peak lags that at the protein. This delay is the time required for the heat to diffuse from the interface to the location of the mode peak, a distance of roughly $0.5 \mu\text{m}$ according to the Fig. 5.2. The calculated time delay of $\tau_{delay} \approx 0.8 \mu\text{s}$ corresponds well to the value of τ_{HT} estimated above, although it should be noted

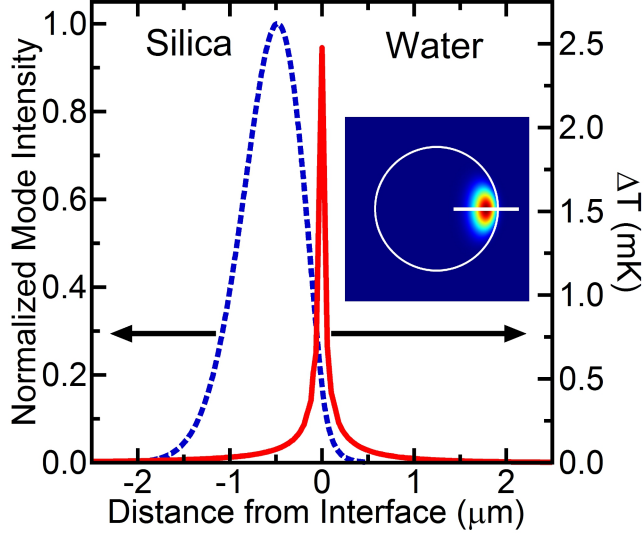


Figure 5.4: The normalized mode profile in a toroidal resonator with major radius $r_a = 40 \mu\text{m}$ and minor radius $r_i = 2.5 \mu\text{m}$ corresponding to the shown cut line (inset) and the thermal plume resulting from a single-molecule protein heat source exposed to a mode with $Q = 10^8$ and $P_D = 1 \text{ mW}$ resulting in linear absorption by the molecule.

that these simple scaling arguments do not capture the full complexity of the interactions of the thermal plume with the optical mode. This plume may also lead to localized thermal expansion of the resonator and affect sensor response. Modeling the thermal expansion near the protein, we conclude that the temperature rise that results from linear absorption is too small to measurably affect the resonance shift and omit it from further calculations.

We can now estimate the resonance shift by integrating over the calculated 3-dimensional temperature profile according to Eq. (5.14). This integral is evaluated at each time point for a range of quality factors, as shown in Fig. 5.6. The predicted shifts in resonant wavelength for Q values ranging from 10^6 to 10^8 fall between 0.05 to 1.6 am (10^{-18} m), as indicated by the maxima in the curves of Fig. 5.6. The resonance shift corresponding to $Q = 10^8$ is a factor of $10^3 - 10^4$ smaller than the sensor responses observed in SM1 and SM2, suggesting that linear absorption by the protein in the absence of bulk heating is insufficient to explain those experimental results. However, while decreasing Q may also decrease the intensity of the protein heat source, it extends the time power is coupled into the resonator and the duration of the heat pulse. This produces a nonlinear relationship between Q and $\Delta\lambda_R$, and a deviation from power law behavior in the inset

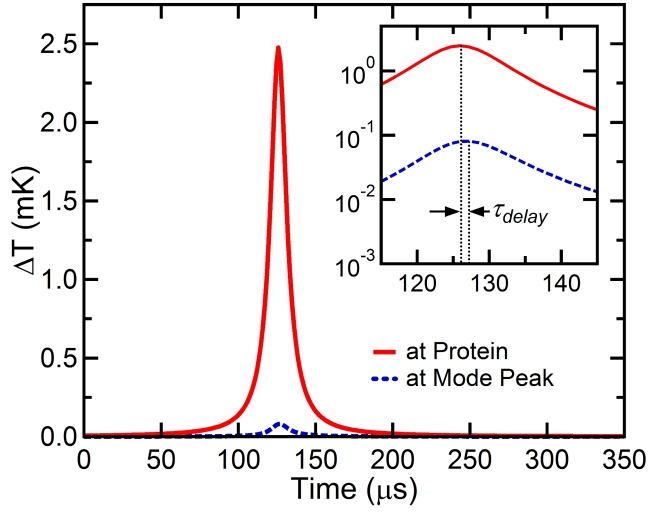


Figure 5.5: The temperature at the location of the protein (red) and mode peak (blue) as a function of time where the only heating comes from a protein exhibiting linear absorption bound to the surface of the toroidal sensor with $Q = 10^8$, $P_D = 1$ mW, and $\frac{d\lambda}{dt} = 1.35$ nm s $^{-1}$.

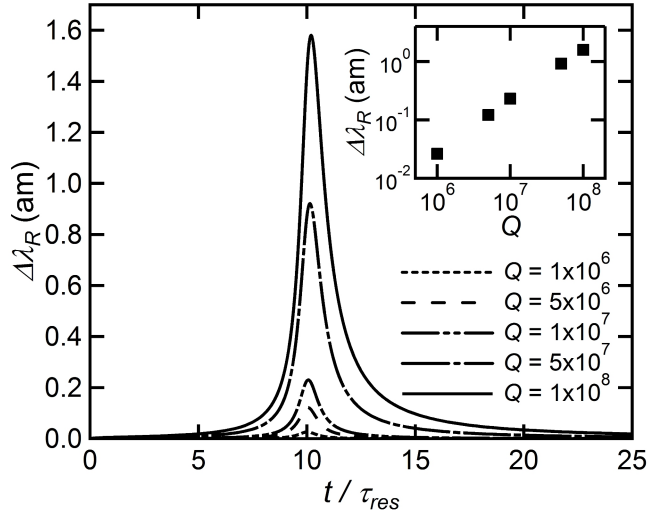


Figure 5.6: The resonance shift due to a single-molecule protein heat source for toroidal resonators ($r_a = 40$ μm , $r_i = 2.5$ μm) with $P_D = 1$ mW and $\frac{d\lambda}{dt} = 1.35$ nm s $^{-1}$ for varying quality factor. This shift is plotted against a relative time t/τ_{res} to simplify comparison. The maximum signal is plotted as a function of Q in the inset.

to Fig. 5.6.

We leave for future work the consideration of bulk heating, decreases in Q due to the accumulation of protein on the sensor, and nonlinear optical effects, the latter which pose a variety of challenges. Bulk heating demands that Eq. (5.10) include the first term on the right side of the equation, increasing the computational demands. Consideration of nonlinear optical effects requires additional knowledge about molecular properties that, if available in the literature, are difficult to locate.

5.8 Conclusions

Single-molecule sensitivity in WGM biosensors remains controversial due to the inability to reconcile experimental results with physical models. A review of the models to date reveals an oversimplified physical system and a failure to accurately model the single-molecule experiments. In particular, previous models ignore the exclusively transient nature WGM sensing experiments in the literature, instead adopting a steady-state assumption that precludes relevant physical processes. This time dependence implies that, as the wavelength is scanned during a measurement of λ_R , changes occur in the optical field intensity, the heat generated by the single-molecule source, the temperature profile, and the physical properties of the system. The model presented here incorporates the transient nature of the WGM experiments to predict the observed shift in λ_R , while still making simplifying physical assumptions: (i) the only heat added to the system comes from a protein undergoing linear absorption and (ii) temperature perturbations to the mode structure are negligible. We find that, in the limit of linear absorption by a single protein heat source and consequential thermo-optical effect, even the present, more rigorous model underestimates the reported sensitivity by a factor of $10^3 - 10^4$. Nonetheless, this model lays the groundwork for future studies. Present knowledge of the physical properties of biomolecules bound to the resonator surface limits our ability to model the sensor response. Data on the nonlinear optical coefficients for non-fluorescent proteins are needed, as is a fundamental understanding of energy transfer mechanisms at the single molecule level.

The authors would like to thank the Jacobs Institute for Molecular Engineering for Medicine at the California Insitute of Technology and the NASA Astrobiology Institute through the NAI Titan team managed at JPL under NASA Contract NAS7-03001 for the funding of this project, and the Ayrshire Foundation for their support in making computing resources available.

5.9 Supplemental Information

Finite Element Model

Calculating the 3-dimensional, transient temperature distribution $T(\mathbf{r}, t)$ at position \mathbf{r} and time t that results from a single-molecule heat source at the interface between a toroidal WGM optical resonator and the surrounding medium is challenging. This task requires integrating the energy balance equation for an arbitrary differential volume element, an expression which may be written as

$$\rho C_P \frac{dT}{dt} + \kappa_T \nabla^2 T = \frac{\omega \alpha \lambda n |\mathbf{E}|^2}{2\pi} + h_{SM} \delta(\mathbf{r} - \mathbf{r}_a), \quad (5.12)$$

where ρ is the material density, C_P is the heat capacity, κ_T is the thermal conductivity, and $|\mathbf{E}(\mathbf{r}, t)|$ is the magnitude of the electric field. The right hand side of Eqn. (5.12) represent the generation of heat due to absorption by the bulk materials, i.e., silica and water, (first term) and heat due to absorption by a single-molecule bound to the sensor at position \mathbf{r}_a giving off heat at a rate h_{SM} (second term). Here, δ represents the Dirac function.

Calculations were performed numerically, using the finite element (FE) mathematics software COMSOL Multiphysics 4.2. The present work makes the assumption that the thermal plume created by a single molecule will be small enough that the interface between the resonator and the surrounding medium may be approximated as planar, leading to the geometry drawn in Figure 5.7. The FE method allows the user to concentrate computation power on regions of the geometry over which the equations apply where the dependent variables change rapidly with position by controlling the size of local mesh elements. We take

advantage of this feature by creating numerous subdomains in the geometry, within which the mesh element size is independently described to cut down on computation time by assuming changes in the temperature profile are small near the boundaries of (see Fig. 5.7b). The simulated geometry extends $20\ \mu\text{m}$ into each material and $40\ \mu\text{m}$ in each direction along the interface. A cubic subdomain $3\ \mu\text{m}$ in length was defined at the center of the geometry with a maximum mesh size of $50\ \text{nm}$ and surrounded by a larger cubic domain $6\ \mu\text{m}$ in length with a maximum mesh size of $1\ \mu\text{m}$, which encompassed the entire region where temperature changes due to heating exceeded $10^{-7}\ \text{K}$.

Solving Equation (5.12) requires boundary conditions that are applied to all mesh elements that touch an outer boundary of the geometry. The total volume of the system was large compared to the thermal plume that evolves during the WGM sensing experiment to allow us to apply a boundary condition at the extremities holding temperature constant at the ambient value of $T = 298\ \text{K}$. The boundaries between all other mesh elements was left at their default boundary setting, which COMSOL refers to as *continuity*. This implies that temperature and thermal flux are continuous across each mesh element interface. The point at the center of the geometry, which lies on the interface between silica and water, was designated as a point

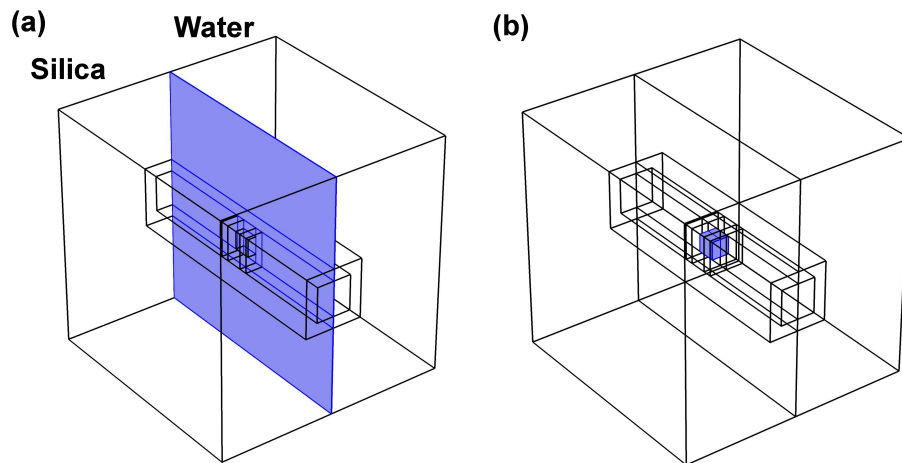


Figure 5.7: The geometry used in COMSOL Multiphysics to solve Eqn. (5.12) for the transient temperature profile resulting from the excitation of a single-molecule heat source located at what is assumed to be a locally planar interface (blue plane) between a toroidal WGM optical resonator and the water surrounding it. The interior lines are boundaries between subdomains created within the geometry to allow for convenient control over local mesh element size, reducing computation time and memory requirements.

source of heat that obeys a transient intensity function of

$$h_{SM} = \frac{\sigma \text{Im}(\mathbf{S} \cdot \hat{\phi}) \tau_{res}^2}{4(t - t_0)^2 + \tau_{res}^2}, \quad (5.13)$$

where σ is the absorption cross-section of the protein, $\text{Im}(\mathbf{S})$ is the imaginary part of the Poynting vector at the position of the protein, $\hat{\phi}$ is the unit vector in the direction of light propagation, t_0 is the time during the wavelength scan when $\lambda = \lambda_R$, and $\tau_{res} = \lambda / (\frac{d\lambda}{dt} Q)$. This expression describes the Lorentzian profile expected in the absence of bulk heating.

Since we considered resonators with varying quality factors, we evaluate the temperature profile over the geometry at a range of times that were scaled according to τ_{res} . The center of the Lorentzian profile was set to occur at $t = t_0 = 10\tau_{res}$ for all cases. For $0 < t < (t_0 - 2\tau_{res})$ and $(t_0 + 2\tau_{res}) < t < 3t_0$, the time resolution of the calculation was set to $\tau_{res}/6$, while time resolution was improved to $\tau_{res}/60$ during the part of the experiment when significant heat was being generated by the protein, i.e., $(t_0 - 2\tau_{res}) < t < (t_0 + 2\tau_{res})$.

In order to calculate the mode profile, we used methods outlined by Oxborrow [103]. This technique, which uses the axial symmetry of a WGM resonator to simplify the calculation, could not be used directly with our assumption of a locally-planar material interface. We instead mapped the mode onto the planar geometry by using the axisymmetric solution for the mode cross-section as the basis for an interpolation function in the plane normal to propagation and by assuming that the time-averaged mode does not vary in the direction of propagation. The mode profile was used for the weighted calculation of the change in effective refractive index, Δn_{eff} , experienced by the resonant light which may be approximated in terms of the electric field intensity, $|\mathbf{E}(\mathbf{r})|$, using the expression

$$\Delta n_{eff} \approx \frac{\int_V \frac{dn}{dT} \Delta T(\mathbf{r}) |\mathbf{E}(\mathbf{r})| dV}{\int_V |\mathbf{E}(\mathbf{r})| dV}. \quad (5.14)$$

The electric field intensity may be easily calculated from the axisymmetric mode profile [103].

The experimental parameters used to predict the WGM optical biosensor response to the binding of a single protein molecule to the surface of an ultra-high Q toroidal resonator in the absence of bulk heating

or nonlinear optical phenomena are shown in Table 5.3. Material properties for silica and water are also included in Table 5.4.

Thermal Effects in WGM Optical Resonators

Absorption by the resonator and its surrounding medium, though often negligible at low coupled power and low quality factor, can be significant for the ultra high Q WGM optical biosensors for which extreme limits of detection have been reported. The warping of the Lorentzian transmission trough that results from absorptive heating and subsequent thermo-optical resonance shift during the wavelength scan could help explain the sensitivity observed in SM1 and SM2. Though no raw data (i.e., transmission spectra) are available for those studies, we can see how similar conditions in Figure S5.8, which include 2.6 mW coupled into a toroidal resonator in water with $Q \approx 10^7$ at $\lambda = 765$ nm, can produce significant broadening of the transmission trough for positive scan rate and narrowing of the trough for negative scan rate. This implies that the methods described above, which assume a Lorentzian time profile for the transient point source of heat, may significantly underestimate the amount of heat put into the system. If taken with a positive wavelength scan rate, data collected during a sensing experiment may be influenced by a heat source with a lifetime that could be orders of magnitude longer than τ_{res} .

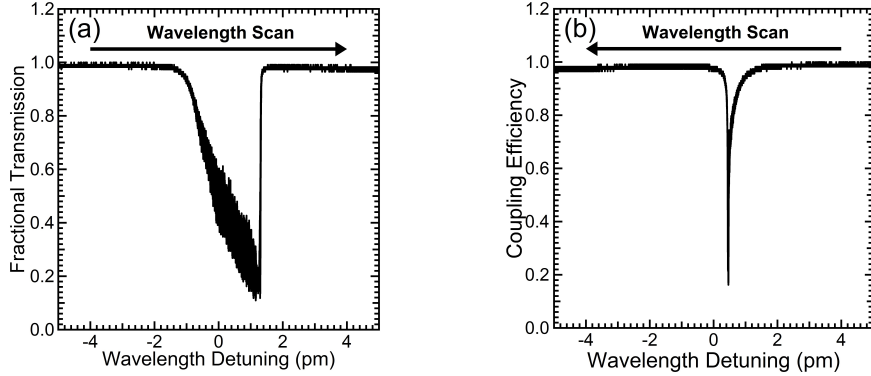


Figure 5.8: Transmission spectrum for a toroid of major radius $r_a = 40 \mu\text{m}$ and minor radius $r_i = 5 \mu\text{m}$ and $Q \approx 10^7$ at wavelength scan rates of (a) $\frac{d\lambda}{dt} = 7.6 \text{ nm/s}$ and (b) -7.6 nm/s . The resonator is submerged in water and is being excited using a 765 nm external cavity tunable laser, with a maximum coupled power of 2.6 mW. The difference in resonance linewidth and transmission minimum is due to thermal distortion of the Lorentzian trough, where λ_R shifts during the scan when light is absorbed and the system warms. Since this warming results in a red shift of λ_R , a positive scan rate leads to an artificially broad line and a negative scan rate yields an artificially narrow line.

Table 5.3: Experimental Parameters for Modeling WGM Biosensing Experiment

Parameter	Symbol	Value
Quality factor	Q	1×10^8
Driving power	P_D	1 mW
Wavelength scan rate	$\frac{d\lambda}{dt}$	$1.35 \frac{\text{nm}}{\text{s}}$
Wavelength Scan Duration	τ_{scan}	5 ms
Driving pulse FWHM	τ_{res}	5 μs
Energy flux at the protein	$\text{Im}(\mathbf{S})$	$6 \times 10^{13} \frac{\text{W}}{\text{m}^2}$

Table 5.4: Physical Properties of Silica and Water at 298 K and 680 nm

Property	Symbol	Units	Silica	Water
Thermal Conductivity	κ_T	$(\frac{\text{W}}{\text{m}\cdot\text{K}})$	1.38 [137]	0.58 [137]
Density	ρ	$(\frac{\text{kg}}{\text{m}^3})$	2203 [137]	997 [137]
Heat Capacity	C_p	$(\frac{\text{J}}{\text{kg}\cdot\text{K}})$	703 [137]	4186 [137]
Thermo-Optical Coefficient	$\frac{dn}{dT}$	$(\frac{1}{\text{K}})$	1.3×10^{-5} [1]	-9.9×10^{-5} [135]
Refractive Index (Real)	n		1.4694 [110]	1.33322 [138]
Refractive Index (Imaginary)	k		1.74×10^{-10} [139]	1.41×10^{-8} [140]
Absorption Coefficient	α_{abs}	$(\frac{1}{\text{m}})$	0.0034 [139]	0.28 [140]